Int. J. Electrochem. Sci., 7 **(2012)** 5734 - 5745

International Journal of ELECTROCHEMICAL SCIENCE
www.electrochemsci.org

Synthesis and Some Physical Properties of Magnetite (Fe_3O_4) Nanoparticles

H.El Ghandoor[1], H. M. Zidan[2], Mostafa M.H. Khalil[3] and M. I. M. Ismail[4,]*

[1] Physics Department, Faculty of Science, Ain Shams University, Cairo 11566, Egypt
[2] Physics Department, Faculty of Science, Mansora University-Damietta Branch, New Damietta, Egypt
[3] Chemistry Department, Faculty of Science, Ain Shams University, Cairo 11566, Egypt
[4] Physics Department, Faculty of Engineering, Suez Canal University, Ismailia, Egypt
[*]E-mail: Muhammad_398@yahoo.com

Received: 5 December 2011 / *Accepted:* 4 April 2012 / *Published:* 1 June 2012

Fe_3O_4 nanoparticles and non aqueous stable magnetic fluid (MF) containing Fe_3O_4 nanoparticles with mean diameters of 10 nm, which are in the range of super-paramagnetism, are prepared. Magnetite nanoparticles are synthesized via co-precipitation method from ferrous and ferric solutions. X-ray diffraction (XRD), transmission electron microscopy (TEM) and vibrating sample magnetometer (VSM) are used to study the physical properties of the (MF) and powder. The band gap parameters of the magneto-nanopowders such as the direct, indirect-band gap energies, Fermi energy and Urbach energy are determined.

Keywords: Co-precipitation; Magnetic; Nanomaterial; Optical property.

1. INTRODUCTION

Many authors prepared Magnetite its different properties, but still Magnetite inspire researcher's new researchable ideas, this due to its characteristics, which has a great significance in various fields. Especially, when this material in a nano - size. For example, Magnetite (Fe_3O_4) nanoparticles have attracted much interest not only in the field of magnetic recording media such as audio and videotape, and high-density digital recording disks, magnetic fluids, data storage, but also in the areas of medical care such as drug delivery systems (DDS), medical applications, including radio-frequency hyperthermia, photomagnetics, and magnetic resonance imaging (MRI), medical diagnostics and cancer therapy and microwave devices, magneto-optics devices, sensors, high frequency applications, catalysis and magnetic sensing [1-11].

Authors used to prepare (Fe_3O_4) as pure phase [12 - 15] or ($M_xFe_{3-x}O_4$) by changing the ratio between Fe/M [16], where M any bivalent metal, but in this work, Fe_3O_4 nanoparticles and MF were prepared by chemical co-precipitation method, where the chemical co-precipitation method was adopted a new source of ferrous which is $(NH_4)_2Fe(SO_4)_2$, the ratio between Fe^{+2} and Fe^{+3} is 1:2.

Fe_3O_4 nanoparticles were investigated by X-ray diffraction (XRD) to determine the sample phases and average particle size of the dried powders, the microstructure and the particle size were determined by transmission electron microscopy (TEM), magnetization measurements were done at room temperature up to a maximum magnetic field (H) of 900 Tesla by using VSM homemade and magnetic parameters like specific saturation magnetization (Ms), coercive force (Hc) and remanence (Mr) were evaluated.

Based on a review of the existing literature, data on band gap of magneto nanoparticles is yet scanty; therefore analysis of the different band gap parameters is conducted on the form of MF.

Finally, the optical absorption of the magnetic nanoparticles in the form of MF was measured to determine optical parameters such as optical energy band gap of indirect and direct transition occurring in band gap, Urbach energy and Fermi energy.

2. EXPERIMENTAL PROCEDURES

2.1. Synthesis of Fe_3O_4 nanoparticles

The magnetization of substituted ferrite nanoparticles synthesized by co-precipitation method depends mostly on parameters such as reaction temperature, pH of the suspension, initial molar concentration, etc. [12]. Ultra fine particles of Fe_3O_4 are prepared by co-precipitating aqueous solutions of $(NH_4)_2Fe(SO_4)_2$ and $FeCl_3$ mixtures, respectively, in alkaline medium. $(NH_4)_2Fe(SO_4)_2$ and $FeCl_3$ solutions are mixed in their respective stoichiometry (i.e, ratio Fe^{+2}: Fe^{+3} = 1:2). The mixture is kept at 80 ^oC. This mixture is added to the boiling solution of NaOH (0.5 mol. is dissolved in 600 ml of distilled water) within 10 second under constant stirring. Magnetite is formed by conversion of metal salts into hydroxides, which take place immediately, and transformation of hydroxides into ferrites. The solution is maintained at 100 ^oC for 1.5 h.

The Fe_3O_4 particles are washed several times by distilled water then are divided into three parts. In the first part, the Fe_3O_4 particles are remained in the distilled water without any additives as prepared, in the second part, the Fe_3O_4 particles are just dried at 100 ^oC for 1 h and the third part is centrifuged then is redispersed in oleic acid, oleic acid works as a liquid carrier, this step in order to prepare the MF from the nanoparticles of Fe_3O_4.

2.2. Characterizations of MF nanoparticles

The first part of Fe_3O_4 was used to study the microstructure and determine the particle size by transmission electron microscopy (Jeol_Jem_1230 electronmicroscope).

The second part was analyzed using X-ray diffraction (Philips X'Pert, CuKa, 40 kV, 30 mA and k = 1.54056 Å) to determine the sample phases and average particle size of the dried powder. The magnetization measurements were done at room temperature up to a maximum magnetic field (H) of 900 Tesla by using VSM homemade and parameters like specific saturation magnetization (Ms), coercive force (Hc) and remanence (Mr) were evaluated.

The third part was tested by spectrophotometer (Unicam UV-2) to record the optical absorption of the Fe_3O_4 particles in the form of MF, by the optical absorption results; it is possible to determine each of optical energy band gap of indirect and direct transition occurring in band gap, Urbach energy and Fermi energy.

3. RESULTS AND DISCUSSION

3.1. X-ray powder diffraction analysis

The X-ray diffraction patterns of the dried sample are shown in Fig. 1.

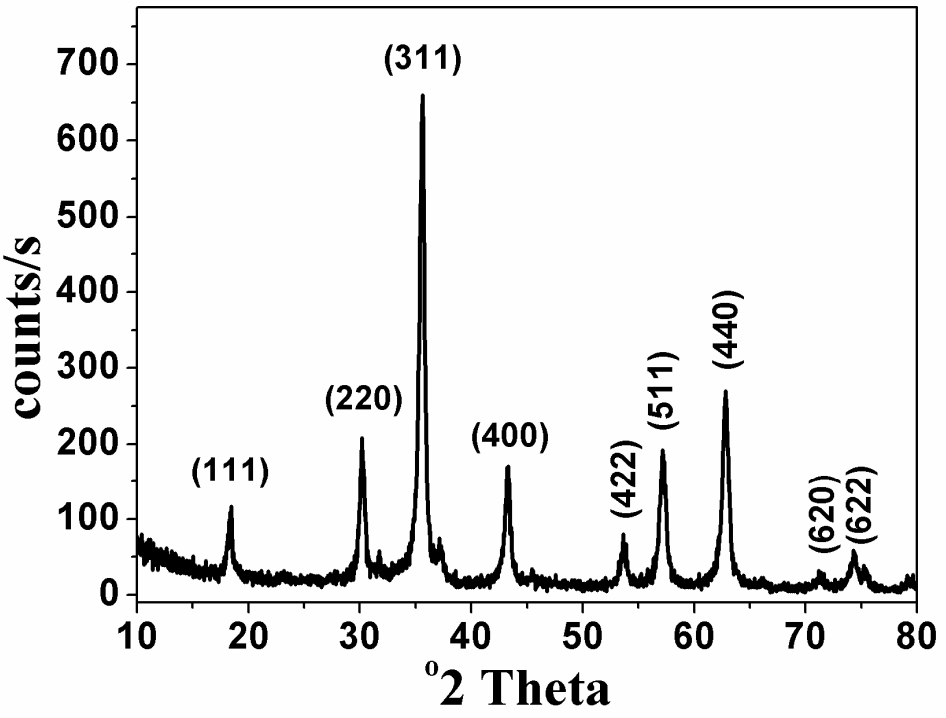

Figure 1. X-ray diffraction pattern of the prepared Fe_3O_4 particles

It can be seen that, the sites and intensity of the diffraction peaks are consistent with the standard pattern for JCPDS Card No. (79 - 0417) Magnetite - synthetic. The sample show very broad peaks, indicating the ultra-fine nature and small crystallite size of the particles. Cubic single phase

nano sized Fe_3O_4 powder has been obtained. According to the Debye–Scherrer formula, the crystallite size D_{hkl} for the sample is given by [13].

$$D_{hkl} = \frac{0.9\lambda}{\beta \cos\theta} \qquad (1)$$

Where β is the full-width at half-maximum (FWHM) value of XRD diffraction lines (see Fig. 1), the wavelength λ = 0.154056 nm and θ is the half diffraction angle of 2θ. The particle size is determined by taking the average of the sizes at the peaks D_{220}, D_{311}, D_{400}, D_{422}, D_{511} and D_{440}. And it was found to be 10 nm. The lattice parameter "a" and interplanar spacing d_{hkl} are determined by Eq. (3) Bragg's law (Eq. (2)) [14]. The values obtained are shown in Table 1:

$$d_{hkl} = \frac{\lambda}{2 \sin\theta} \qquad (2)$$

$$d_{hkl} = \frac{a}{\sqrt{h^2 + k^2 + l^2}} \qquad (3)$$

Table 1. Interplanar spacing, lattice Parameter, (XRD and TEM) of Fe_3O_4.

sample	Interplanar spacing d_{hkl} (Å)	Lattice parameter "a_o" (Å)	Crystallite size estimated from	
			XRD (nm)	TEM (nm)
Fe_3O_4	2.5092	8.322	10.0	10.59

The lattice parameter and interplanar spacing for the prepared sample is lower than the values reported for bulk magnetite JCPDS Card No. (79-0417) (a = 8.394 and d_{311}= 2.531), but these values are closed to the values in some references as in [17-19]. The values which are obtained for the sample can be attributed to simultaneous formation of another phase such as γ-Fe_2O_3 (a = 8.347 and d_{311} = 2.517) [17].

The information regarding lattice strain is calculated from the full-width at half-maximum (FWHM) of diffraction peaks. The relation between particle size and strain is estimated using the following equation:

$$\frac{\beta \cos\theta}{\lambda} = \frac{1}{\varepsilon} + \frac{\eta \sin\vartheta}{\lambda} \qquad (4)$$

where β is a measurement of FWHM in radians, θ is Bragg angle of the diffraction peaks, λ is the wavelength of the X-rays used, ε is the effective particle size and η is the amount of strain [19].

Fig. 2 shows the variation of $(\beta \cos\theta)/\lambda$ with $(\sin\theta)/\lambda$ for the Magnetite sample.

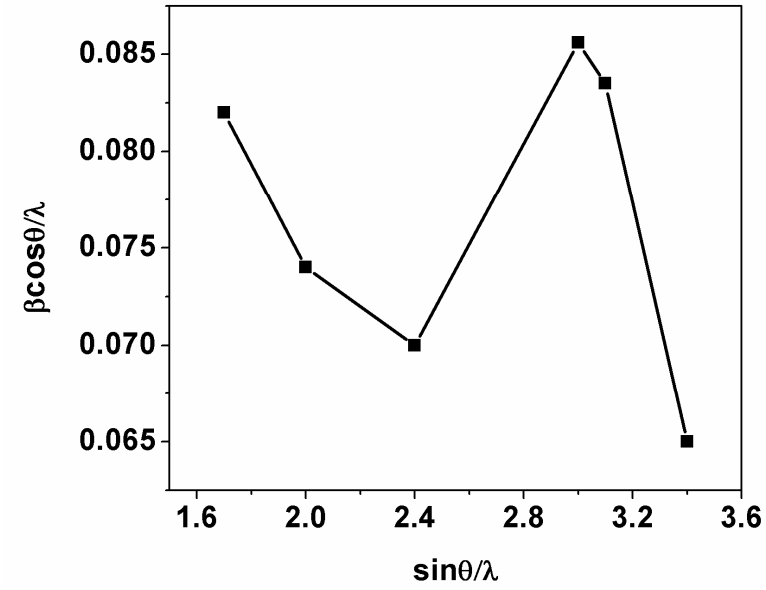

Figure 2. βcosθ/λ versus sinθ/λ for Fe_3O_4 particles.

3.2. Transmission electron microscopy

The morphology of the magnetite particles formed is examined by direct observation via high-resolution transmission electron microscopy for all the collected particles. The micrograph of Fe_3O_4 is given in Figure 3. It is cleared that the tested particles are spherical in shape with a narrow size distribution and their particle sizes are 10.59 nm which is approximately the size calculated by the Debye–Scherrer formula.

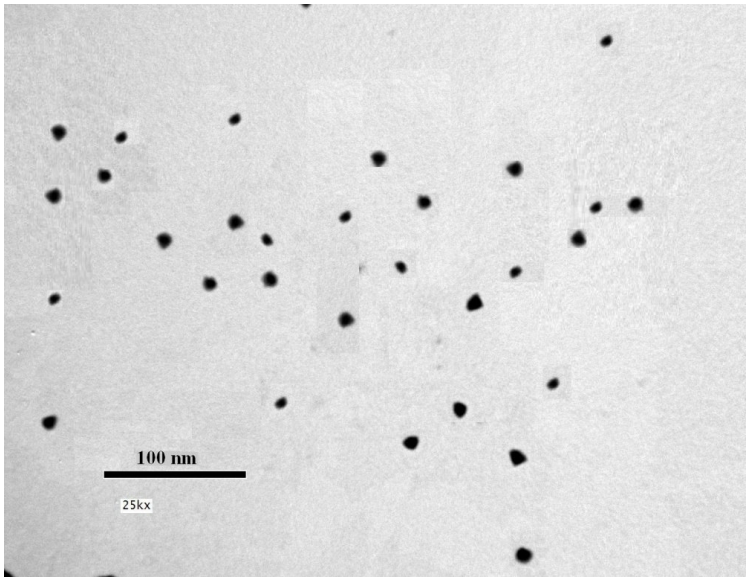

Figure 3. Transmission electron micrograph of Fe_3O_4, the particles are in spherical shape and extremely narrow sized distribution.

3.3. Magnetic characterizations

Figure 4 shows the magnetization, M(emu/g), as a function of the applied magnetic field, H(Oe), the coercivity (H_c), the remanent magnetization (M_r) and saturation magnetization (M_s) of the present sample is determined from Figure 4 and their values are listed in Table 2.

Table 2. Magnetic properties of Fe_3O_4.

sample	M_S (emu/g)		M_R (emu/g)		H_C (Oe)	
	Present work	Published in reference	Present work	Published In reference	Present work	Published in reference
Fe_3O_4	46.7	46.7 [24]	1.65	-	0	8.8 [24]

According to Table 2, M_s is obviously smaller than that of its bulk value, which can be attributed to the disorder canting spins (spin-glass-like) on the surfaces due to the coordination-number imperfection [17-19].

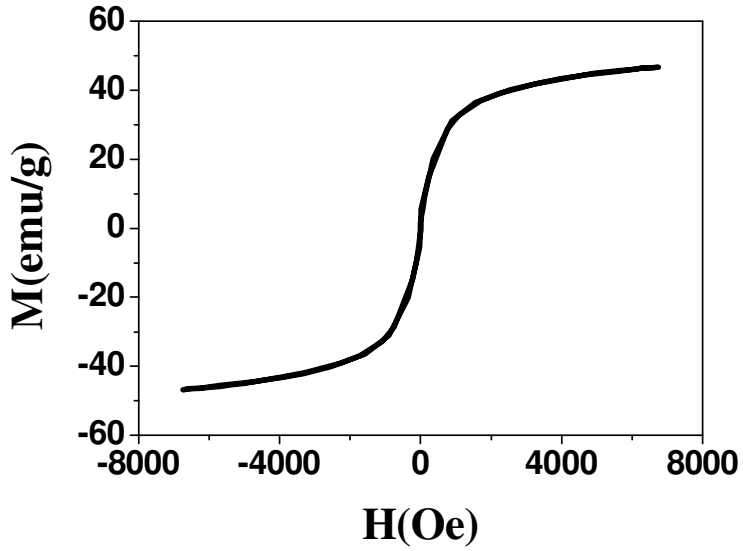

Figure 4. The relation between the applied magnetic field (H) (Oe) and the magnetization (M) (emu/g) of Fe_3O_4 nanoparticles.

It can be readily observed that the smaller particle sizes exhibit smaller values of Ms as expected due to the surface disorder and modified cationic distribution [20]. In other words, the

decrease in Ms at smaller sizes is attributed to the pronounced surface effects in these nanoparticles. The surface of the nanoparticles is considered to be composed of some canted or disordered spins that prevent the core spins from aligning along the field direction resulting in decrease of the saturation magnetization of the small sized nanoparticles [21].

Figure 4 shows that there is no hysteresis loop, $H_c = 0$ Oe**,** this means the super paramagnetic nature of this sample. Superparamagnetic nanocrystals are believed to be promising for wide engineering applications, such as drug delivery, bioseparation and magnetic resonance imaging [22]

The present results are compared with the literature [23, 24] to have a wider view and a deeper insight into the results, and it is found that M_s value is exactly equal to that in the reference [24].

3.4. Spectrophotometric measurements of MF

Figure 5 shows the optical absorption (A) of MF of Fe_3O_4 which is measured in a scanning range of wavelength from 190 to 1000 nm, with scan interval of 0.2 nm. By the optical absorption result, it is possible to determine each of optical energy band gaps of indirect and direct transition occurring in band gap, Urbach energy and Fermi energy as following:

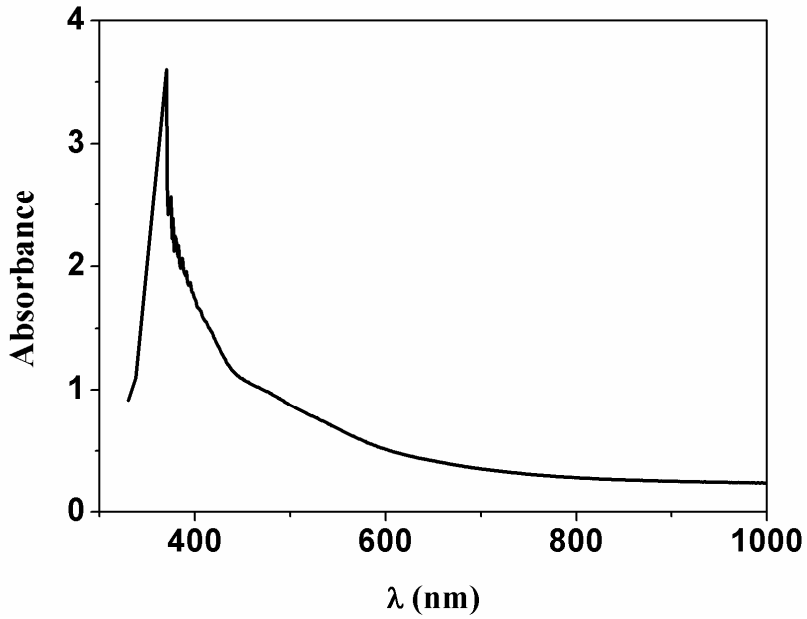

Figure 5. Absorbance A versus wavelength λ (nm) of MF Fe_3O_4.

3.4.1. Determination of optical energy band gap of indirect and direct transition of different MF

Davis and Mott [25] gave an expression for the absorption coefficient, $\alpha(\nu)$, as a function of photon energy ($h\nu$) for indirect and direct transition through the following Eq.

$$A = -\ln(I/I_0) = \alpha(\nu)L \qquad (5)$$

$$\alpha(\nu) = A / L \quad (6)$$

$$\alpha(\nu) = \alpha_0 (h\nu - E_g^{opt})^n / h\nu \quad (7)$$

where A is the absorption, I is intensity of transmitted light, I_o is intensity of incident light, $\alpha(\nu)$ is the absorption coefficient of the sample, L is the thickness of the cell, α_0 is constant related to the extent of the band tailing, E_g^{opt} is optical band gap energy and the exponent n = 1/2 for allowed direct transition, while n = 2 for allowed indirect transition.

By plotting $(h\nu\alpha)^{1/2}$ and $(h\nu\alpha)^2$ as a function of photon energy $(h\nu)$, the optical energy band gap for indirect E_{g2}^{opt} and direct E_{g1}^{opt} transition can be determined, respectively.

The respective values of E_g^{opt} are obtained by extrapolating to $(h\nu\alpha)^{1/2} = 0$ for indirect transition and $(h\nu\alpha)^2 = 0$ for direct transition as shown in Figures 6 and 7, respectively. The results are listed in Table 3.

Table 3. Optical parameters.

X (mol)	E_{g2}^{opt} (eV)		E_{g1}^{opt} (eV)		E_U (eV)		E_F (eV)	
	Present work	Published In reference	Present work	Published in reference	Present work	Published in reference	Present work	Published in reference
Fe_3O_4	1.92	5 [27]	2.87	5.5[27]	0.70	0.53[27]	3.64	5.7[27]

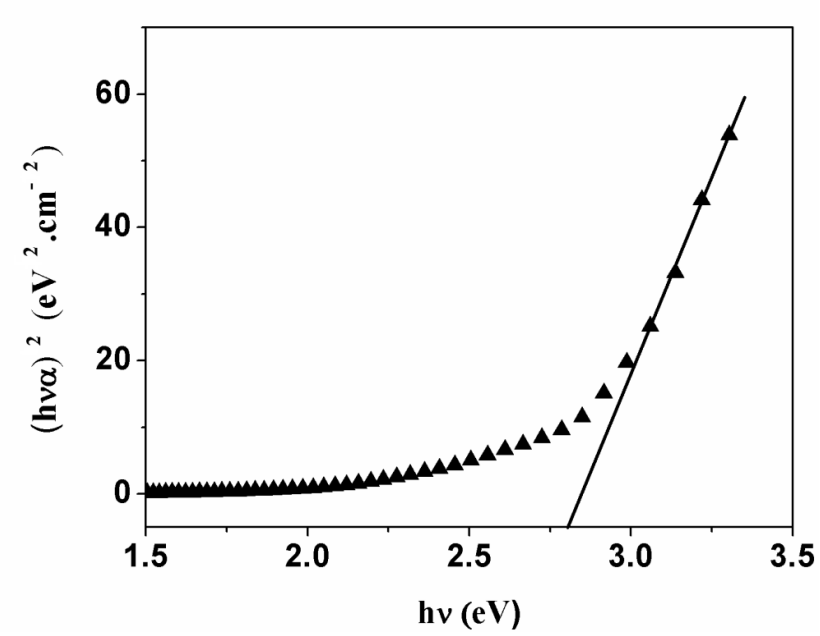

Figure 6. Determination of the optical energy band gap for direct transition E_{g1}^{opt} of Fe_3O_4 MF.

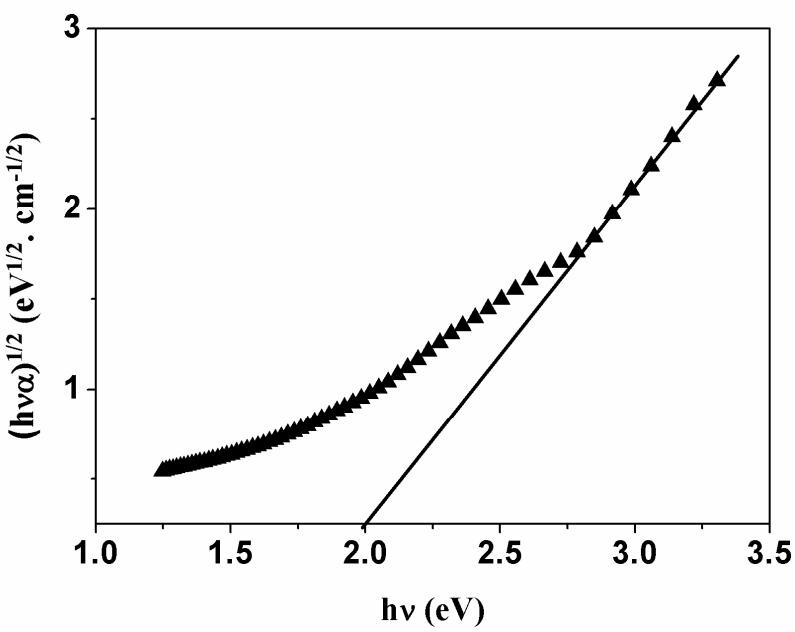

Figure 7. Determination of the optical energy band gap for indirect transition E_{g2}^{opt} of Fe_3O_4 MF.

The goodness of the fit of the data to the formula for either $n = 1/2$ or $n = 2$ is determined by the correlation coefficient ($R^2 = 1$is for the perfect fit) which in our case 0.997. From the values of R^2 it is difficult to decide whether MF has direct or indirect band gap. However, it may be noted that the direct band gap value is larger than the corresponding indirect band gap value.

Table 3 is shown that the values of direct and indirect energy band gaps of Magnetite are less than that in the reference [26] this due to the difference in size, Magnetite in reference has size around 5 nm but in the present work 10 nm, this means that, the energy band gap of the nano materials are inverse proportional to their sizes. By this result, it is easy to say that the energy band gaps of nano materials can be controlled by controlling their sizes.

The values of both direct and indirect energy band gap of the Magnetite sample are classified this sample as a semiconductor, semiconductor energy band gap (0 - 3 eV) [28]. This is a novel result.

3.4.2. Determination of Urbach energy of MF

The Urbach energy characterizes the extent of the exponential tail of the absorption edge and depends on temperature, thermal vibrations in the lattice, induced disorder, static disorder, strong ionic bonds and on average photon energies. The main factor contributing to edge broadening in the crystalline materials is exciton-phonon coupling (dynamic disorder) [29]. The exponential absorption tails and Urbach energy is given in accordance with the empirical relation [30]

$$\alpha(\nu) = \beta \exp(h\nu / E_U) \qquad (8)$$

where β is constant, E_U is the Urbach energy which indicates the width of the band tails of the localized state and (ν) is the frequency of the radiation.

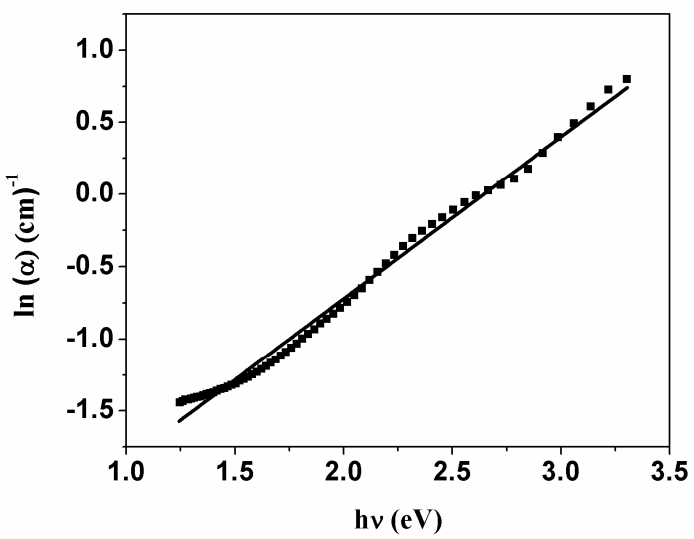

Figure 8. The logarithm of the absorption coefficient, ln(α), against photon energy, ($h\nu$), for Fe_3O_4 MF.

By plotting the logarithm of the absorption coefficient, ln(α), against photon energy, ($h\nu$), for Fe_3O_4 MF Figure 8. Urbach energy of Fe_3O_4 MF sample is calculated by tacking the reciprocals of the slope of the liner portion in the lower photon energy of this curve.

Figure 8 is shown that Urbach energy of Fe_3O_4 sample is 0.7 eV which is larger than that in the reference 0.53 eV [26], this difference in Urbach energy may be refers to the difference in their particle sizes. This means that the present samples are more conducting than that in the reference.

3.4.3. Determination of Fermi energy of MF

Figure 9 shows that, the functions $k(\lambda)$ have step edges toward the UV of the spectrum. If $F(E)$ refers to the maximum absorption value in the UV-absorption edge, thus, the Fermi energy level can be calculated applying the Fermi-Dirac distribution function [31]

$$F(E) = \frac{1}{1+\exp\left(\frac{E_F - E}{K_B T}\right)} \qquad (9)$$

where E_F is the Fermi Energy, E is the variable photon energy, and K_B is the Boltzmann constant. T is the absolute temperature at the moment of measuring the sample spectrum. The calculated values of Fermi energy of MF Fe_3O_4 is 3.64 eV, but the present results are less than that in

reference 5.7 eV[26], this means that the present samples are more conducting than that in the reference.

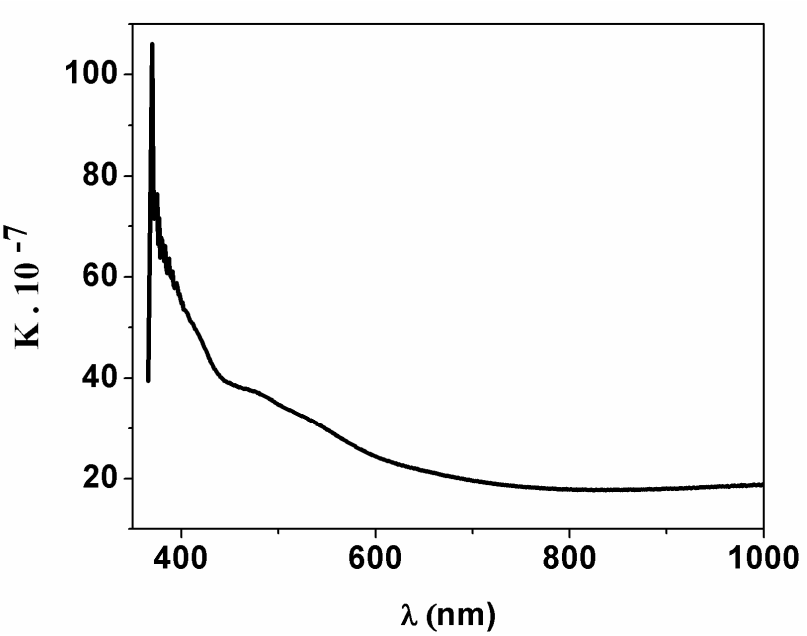

Figure 9. Absorption index versus wavelength of Fe_3O_4 MF.

4. CONCLUSION

Fe_3O_4 nanoparticles and magnetic fluid less than 20 nm are prepared by chemical co-precipitation method, the magnetization measurements are done by using VSM and magnetic parameters like specific saturation magnetization (Ms), coercive force (Hc) and remanence (Mr) are evaluated, from Ms result the sample is consider to be superparamagnet and has no hysteresis loop.

MF is prepared to facilitate spectrophotometric measurements, spectrophotometric measurements and results show that both indirect and direct optical energy band gap are classified the sample as semiconductor materials, and this is a novel result. Both of Urbach and Fermi energy results are supported the semiconductor nature of the prepared magnetite.

References

1. Juliana B. Silva, Walter de Brito, Nelcy D.S. Mohallem, *Materials Science and Engineering* B. 112 (2004) 182.
2. S. Sun, C.B. Murray, D. Weller, L. Folks, A. Moser, *Science* 287 (2000) 1989.
3. S. Sun, *Adv. Mater*. 18 (2006) 393.
4. Q.A. Pankhurst, J. Connolly, S.K. Jones, J. Dobson, *J. Phys. D Appl. Phys*. 36 (2003) 167.
5. T. Neuberger, B. Schöpf, H. Hofmann, M. Hofmann, B. von Rechenberg, *J. Magn. Magn. Mater*. 293 (2005) 483.

6. D. Portet, B. Denizot, E. Rump, J.J. Lejeune, P. Jallet, *J. Colloid Interface Sci*. 238 (2001) 37.
7. A. Ito, M. Shinkai, H. Honda, T. Kabayashi, *J. Biosci. Bioeng*. 100 (2005) 1.
8. X. Meng, H. Li, J. Chen, L. Mei, K. Wang, X. Li, *J. Magn. Magn. Mater*. 321 (2009) 1155.
9. Z. Zi, Y. Sun, X. Zhu, Z. Yang, J. Dai, W. Song, *J. Magn. Magn. Mater*. 321 (2009) 1251.
10. L.X. Phua, F. Xu, Y.G. Ma, C.K. Ong, Thin Solid Films, *Thin Solid Films*. 517 (2009) 5858.
11. E. Kashevsky, V.E. Agabekov, S.B. Kashevsky, K.A. Kekalo, E.Y. Manina, I.V. Prokhorov, V.S. Ulashchik, *Particuology* 6 (2008) 322.
12. Lacava Z, Azevedo R, Martins E, Lacava L, Freitas M, Garcia V, et al. *J. Magn. Magn. Mater*. 16 (1999) 201.
13. Berrington de Gonzalez A.; *Darby S. Lancet*. 363 (2004) 345.
14. B.D. Cullity, S.R. Stock, Elements of X-ray Diffraction, New Jersey,2001.
15. N. Moumen, M.P. Pileni, *Chem. Mater*. 8 (1996) 1128.
16. X. Li, G. Chen, Y. Po-Lock, C. Kutal, *J. Mater. Sci. Lett*. 21 (2002) 1881.
17. Victoria L. Calero-DdelC, Carlos Rinaldi. *J. Magn. Magn. Mater*. 314 (2007) 60.
18. Yue Zhang, ZhiYang, DiYin, YongLiu, ChunLongFei, RuiXiong, JingShi, GaoLinYan. *J. Magn. Magn. Mater.* 322 (2010) 3470.
19. Vinod Kumar, Anu Rana, M.S. Yadav, R.P. Panta. *J. Magn. Magn. Mater*. 320 (2008) 1729.
20. B.P. Rao, O. Caltun, W.S. Cho, Chong-Oh Kim, Cheol Gi Kim, *J. Magn. Magn. Mater*. 310 (2007) 812.
21. K. Maaz, S. Karim, A. Mumtaz, S.K. Hasanain, J. Liu, J.L. Duan, *J. Magn. Magn. Mater*. 321 (2009) 1838.
22. C. Hu, Z. Gao, X. Yang, *J. Magn. Magn. Mater*. 320 (2008) 70.
23. Hironori Iida, Kosuke Takayanagi, Takuya Nakanishi, Tetsuya Osaka, *Journal of Colloid and Interface Science,* 314 (2007) 274.
24. G. Vaidyanathan, S. Sendhilnathan, R. Arulmurugan, *J. Magn. Magn. Mater*. 313 (2007) 293.
25. E. A. Davis, N. F. Mott, *Phil. Mag*. 22 (1970) 903.
26. Fouad El-Diasty, H.M. El-Sayed, F.I. El-Hosiny, M.I.M. Ismail, *Current Opinion in Solid State and Materials Science*, 13 (2009) 28.
27. Rajendra S. Gaikwad, Sang-Youn Chae, Rajaram S.Mane, Sung-Hwan Han, and Oh-Shim Joo, *International Journal of Electrochemistry*, 2011 (2011) 1.
28. W. H. Strehlow and E. L. Cook,*J. Phys. Chem*., 2 (1973) 1.
29. M. Abdel-Baki, F. El-Diasty and F. A. Abdel-Wahab, *Opt. Comm*. 261 (2006) 65.
30. M.A. Hassan, C.A. Hogarth, *J. Mater. Sci*. 23 (1988) 2500.
31. M.A Khashan, A.M. El-Naggar, *Ipt. Commun*. 174 (2000) 445.